Submitted to *Physics of Plasmas*, 2014

Magnetic antenna excitation of whistler modes. 2. Antenna arrays

R. L. Stenzel and J. M. Urrutia

Department of Physics and Astronomy,

University of California, Los Angeles, CA 90095-1547

Abstract

The excitation of whistler modes from magnetic loop antennas has been investigated experimentally. The field topology of the excited wave driven by a single loop antenna has been measured for different loop orientations with respect to the uniform background field. The fields from two or more antennas at different locations are then obtained by superposition of the single-loop data. It is shown that an antenna array can produce nearly plane waves which cannot be achieved with single antennas. By applying a phase shift along the array, oblique wave propagation is obtained. This allows a meaningful comparison with plane wave theory. The Gendrin mode and oblique cyclotron resonance are demonstrated. Wave helicity and polarization in space and time are demonstrated and distinguished from the magnetic helicity of the wave field. The superposition of two oblique plane whistler modes produces in a "whistler waveguide" mode whose polarization and helicity properties are explained. The results show that single point measurements cannot properly establish the wave character of wave packets. The laboratory observations are relevant for excitation and detection of whistler modes in space plasmas.

PACS numbers: 52.35.Hr Electromagnetic waves, 52.50.Dg Plasma sources, 52.40.Fd Plasma interactions with antennas, 94.80.+g Instrumentation for space plasma physics, 94.05.Rx Experimental techniques and laboratory studies

I. INTRODUCTION

Most experiments on whistler mode excitation or detection use electric or magnetic dipoles antennas [1, 2, 3, 4, 5, 6]. In active space plasma experiments, large magnetic loop antennas have not been successfully deployed [7]. However, loop antennas are standard in helicon plasma sources [8, 9, 10]. Dipole antennas do not produce plane waves, yet the basic theories for whistler modes are formulated for plane waves. It would thus be desirable to develop antennas which excite and receive plane waves. The present work suggests that antenna arrays can solve this problem. Unlike arrays in free space, the present antennas do not produce narrow radiation patterns by interference, but the closely spaced array elements impose a wavenumber along the array. The wavenumber vanishes for equal phasing of all array elements. When the array is perpendicular to $\mathbf{B}_0$, it excites plane waves propagating along $\mathbf{B}_0$. With a phase delay along the array, the wave propagates oblique to $\mathbf{B}_0$. Gendrin modes and waves near the resonance cone can be excited. The polarization and magnetic helicity of oblique whistler modes have been demonstrated. Interference of oblique whistlers has been shown to result in whistler "waveguide modes," i.e., standing waves across $\mathbf{B}_0$ and propagating along $\mathbf{B}_0$. These are the simplest helicon modes and avoid the complications due to radial density gradients, boundaries, surface modes, and ionization effects in helicon devices [8, 9]. The interference leads to magnetic null points. The spatial and temporal polarization changes locally from linear to circular, implying that one cannot obtain the propagation of wavepackets from single point polarization measurements ascommonly done in space plasmas.

This paper is organized as follows: After reviewing the experimental setup in Section II, the observations are shown in Section III for loop arrays across $\mathbf{B}_0$, phased arrays, directional arrays and interference of oblique whistlers which form whistler waveguide modes. The findings are summarized in the Conclusion, Section IV.

II. EXPERIMENTAL ARRANGEMENT

The experiments are performed in a pulsed dc discharge plasma of density $n_e \simeq 10^{11}\ cm^{-3}$, electron temperature $kT_e \simeq 2$ eV, and uniform axial magnetic field $B_0 = 5$ G in a large device shown in Fig. 1 and schematically in Fig. 1 of the companion paper [11]. Whistler

modes are excited with a 4 cm diam loop antenna in the middle of the plasma column. The dipole moment has been aligned either along or across the axial dc field $\mathbf{B}_0$ and the rf field $\mathbf{B}_{\rm rf}$ has been measured for each configuration with a single triple magnetic probe (6 mm diam orthogonal loops). The frequency is chosen at $f = 5$ MHz, or $\omega/\omega_{ce} = 0.357$ when normalized to the electron cyclotron frequency. The field topology is measured in three dimensions (3D) by repeating the experiment under identical conditions. All data are collected with a four-channel digital oscilloscope at a 10 ns time resolution. Since we are interested in the wave field, the free-space field of the antenna is measured in vacuum and subtracted from the total field present in the plasma.

Small amplitude signals are used and the linearity between antenna current and wave field has been established. Under these conditions, the superposition of fields from multiple antennas is justified. Examples of two antennas have been shown in the companion paper [11]. Here we extend this concept to multiple antennas in a line, i.e., antenna arrays. The array axis is perpendicular to the dc magnetic field. The array resembles a line dipole when closely spaced, i.e., two antiparallel line currents. The dipole moment can be along or across $\mathbf{B}_0$. It will be shown that line currents produce wave fields which do not vary in the direction of the line. This result suggests that plane waves can be excited by a two-dimensional array in a plane transverse to $\mathbf{B}_0$.

Phased arrays are produced by a time delay from one array element to the next. It produces a phase shift along the array which leads to a tilt in the phase front of the excited wave. The propagation angle depends on the phase velocity of the whistler mode and the array mode.

III. EXPERIMENTAL RESULTS

A. Linear arrays

We start with the field superposition of an increasing number of identical antennas. The superposition is achieved by initially placing the measured data set in a virtual space. Next, a new copy of the data set is offset vertically and added to the original set. This process is then repeated. Given the density of data points, the smaller offset is equivalent to one-half of the antenna radius, or 1 cm. The largest practical offset is 12 antenna radii (24 cm),

yielding a virtual space that is vertically three times taller that the measured data set. This process is shown in Fig. 2 where contours of $B_y(y, z)$, one of the transverse field component s, are displayed for antenna offsets of 12, six, three, and one antenna radii. The antennas have their dipole axis along the x-direction and orthogonal to $\mathbf{B}_0$. We have chosen to only present the central one-third of the virtual space.

For loops separated by an equivalent of 12 antenna radii, the measured field resembles that of a single loop since it exhibits V-shaped phase fronts. When the separation is halved, i.e., six antenna radii, the superposition yields rippled contours of $B_y = \text{const}$. As the separation is decreased and the number of elements increased, the ripples decrease and the phase front becomes constant in the y-direction. Thus, it is a plane wave in 2D with $(k_y = 0, k_z)$, but it is not yet a plane wave in 3D since $k_x \neq 0$.

It should be noted that this array differs from antenna arrays used in free-space. There, the element spacing must be larger than half a wavelength in order to obtain constructive interference at oblique angles. In the present case, the loops can be stacked closely such that the array approximates a line dipole formed by two antiparallel line currents in the y-direction. Stacking such line dipoles also in the x-direction would yield approximately plane waves.

The field topology of antennas aligned along the y-axis with their dipole moments along $\mathbf{B}_0$ is now explored in a transverse x–y plane at $z = 18$ cm from the antenna arrays. Three antenna separation cases are shown in Fig. 3: (a) 12 antenna radii, (b) six antenna radii and (c) one antenna radius. With the antennas widely separated, the field resembles that of a single loop and exhibits the familiar whistler vortex [12]. Its topology consists of a poloidal or dipole field (B_r, B_z), linked by a toroidal field $(B_x, B_y) = \mathbf{B}_\theta$, shown in a vector field. Right-handed linkage implies positive magnetic helicity, identifying wave propagation along $\mathbf{B}_0$. The magnitude B_{rf}, displayed as a contour plot, as well as B_z, are nearly independent of azimuthal angle θ, similar to the $m = 0$ modes in helicon devices [8, 9].

The fields obtained with a six antenna radii separation show three overlapping vortices resulting in rippled amplitude contours of $B_\perp$. For close stacking of loops the fields become constant along the direction of the array ($k_y \simeq 0$) but there remains a variation along x ($k_x \neq 0$). The vectors change direction and magnitude along x since the phase front is wedge-shaped with decreasing amplitude. In time, the vectors rotate counter clockwise.

The arrays are now stacked in y and x directions in Fig. 4, and the loop dipole moments

are across $\mathbf{B}_0$. For the vertical array, the vectors (B_x, B_y) show no variation along y, hence $k_y = 0$ [Fig. 4(a)] and likewise for the horizontal array $k_x = 0$ [Fig. 4(b)]. For a 2D array, either stacked along the x or y direction, the vectors would be identical throughout the x–y plane, hence the array would excite a plane wave with only $k_z \neq 0$. The contour plots show that the total field strength maximizes in the x–y plane along $x = 0$ as defined by the array. The axial field component vanishes in the x–y plane along $x = 0$ as defined by the array. For a 2D stacked array, $B_z \to 0$ throughout the plane as expected for a plane parallel whistler mode.

Note that a single large loop of the size of the x–y plane would not radiate a plane wave since the antenna field is not uniform and does not easily penetrate into the loop center. Its radiation originates at the wire and exhibits a wide $\mathbf{k}$-spectrum. On the other hand, a loop array provides a uniform antenna field across $\mathbf{B}_0$, provided the array dimensions do not exceed the free space wavelength. It is analogous to a plane grid for exciting plane electrostatic waves. Since whistler modes are right-hand circularly polarized, two phase arrays can provide unidirectional radiation as shown earlier for single antennas. Furthermore, a linear array of smaller loops or a line dipole may be easier to deploy in space than a large loop antenna.

B. Phased arrays

The antenna array could be inclined with respect to $\mathbf{B}_0$ in order to generate oblique whistler modes. However, this can also be accomplished by a phase shift between antenna array elements. The latter produces a wave propagation along the array, which delays the wave excitation along $\mathbf{B}_0$ and results in inclined phase fronts. This effect is demonstrated in Fig. 5 which displays contours of the transverse wave magnetic field B_y for different delays between the stacked loops. In a practical realization of a phased array, the stacking should not be so tight that the loops couple, i.e., the mutual inductance should be small compared to the self inductance.

When all elements radiate in phase ($\Delta t = 0$), the phase fronts are parallel to the y-direction and the wave vector $\mathbf{k}$ points along $\pm\mathbf{B}_0$, However, the linear array along y still has a k_x component. Introducing a phase delay results in inclined phase fronts, i.e., oblique propagation at a phase velocity angle θ between $\mathbf{k}$ and $\mathbf{B}_0$. The vertical wavenumber,

$k_y = \omega/v_y$, is given by the frequency and propagation speed, $v_y = \Delta y/\Delta t$,where Δy is the loop spacing and Δt is the delay time between adjacent loops. The parallel wavenumber is determined by the dispersion relation for oblique whistlers, usually expressed by the refractive index relation $n^2 = (kc/\omega)^2 = 1 + {\omega_{pe}}^2/[\omega(\omega_{ce}\cos\theta - \omega)]$ where ω_{pe} and ω_{ce} are the electron plasma and cyclotron frequency, respectively. The expression slightly simplifies to $n^2 \simeq \omega_{pe}^2/[\omega(\omega_{ce}\cos\theta - \omega)]$ in the high density limit of the present experiment. Thus, as the delay is increased, the angle θ increases, the refractive index $n = c/(f\lambda)$ increases or the wavelength λ decreases as shown in Figs. 5(a-e). Highly oblique waves are observed because the wave packet of the single antenna contains a wide spectrum of perpendicular wave numbers. The vacuum field of the antenna array does not extend far into the plasma to produce oblique modes.

Oblique cyclotron resonance ($n \to \infty$) occurs when $\cos\theta = \omega/\omega_{ce} = 0.357$ or $\theta \simeq 69°$. Figure 5(f) shows that the wave amplitude nearly vanishes making the direction of wave propagation difficult to identify. Further increase of the delay time recovers wave propagation at a negative and decreasing angle until parallel propagation is reached when $\Delta t = 2\pi/\omega$.

The theory for oblique whistler modes is well understood [13], but has not been directly demonstrated experimentally with oblique plane waves. However, it has been shown via spatial Fourier transformation that the components $B(\mathbf{k})$ of whistler vortices are those of oblique plane whistlers [14]. The anisotropic propagation of whistlers is usually summarized by its refractive index surface, $\mathbf{n}(\theta)$. For the experimental parameters, Fig. 6(a) shows a plot of $n_\parallel$ vs $n_\perp$. With $n = c/v_{\text{phase}} = kc/\omega$, the direction of $\mathbf{n}$ is parallel to the phase velocity and the wave vector $\mathbf{k}$. The group velocity v_{group} is normal to the refractive index curve and generally differs from v_{phase} in direction and magnitude. Oblique resonance occurs for $\theta \simeq 69°$ where $\cos\theta = \omega/\omega_{ce}$. Experimentally, $n_\parallel$ and $n_\perp$ are obtained from the wavelengths along and across $\mathbf{B}_0$ in Fig. 5 and a best fit for the plasma frequency ($f_{pe} \simeq 3250$ MHz). The resulting red data points, shown in Fig. 6(a), lie close to the theoretical curve, although deviations can arise from the wave dependence in x-direction.

Figure 6(b) shows oblique wave properties vs delay increment Δt or phase shift $\Delta\phi = 2\pi \times \Delta t/T_{\text{rf}}$, where $T_{\text{rf}} = 1/f = 200$ ns is the rf period. The phase shift introduces a wave propagation in the y-direction with phase velocity $v_y = \Delta y/\Delta t = \omega/k_y$. Thus, the wavenumber varies linearly with time, assumes a peak value $k_y = 2\pi \times 5$ MHz $\times 100$ ns/ 2 cm $= 1.5$ cm^{-1}, reverses sign for $\theta > 90°$ and vanishes at $\Delta t = T_{\text{rf}}$ where the wave propagates

along $\mathbf{B}_0$.

Figure 6(b) also displays the angle of wave propagation, $\theta = \arctan(n_\parallel/n_\perp)$, which rises up to a maximum at the phase velocity resonance. Note that $n_\perp$ is controlled by the phase shift but $n_\parallel$ develops self consistently so as to satisfy the oblique whistler dispersion properties. The latter also affects the wave damping which is indicated by the observed wave amplitude B_y at $y = 0$, $z = 18$ cm from the antenna. The amplitude drops for increasingly oblique propagation and nearly vanishes at the oblique resonance where $\lambda \to 0$. Collisional damping and increasing group velocity angle, i.e., wave spread, contribute to the amplitude loss. Furthermore, the wave energy near the resonance cone is mainly carried by the wave electric field which is not measured by magnetic probes.

Figure 6(c) displays the theoretical relation between the group velocity angle and the phase velocity angle. The group velocity is parallel to $\mathbf{B}_0$ for $\theta_{\rm phase} = 0$ and $\theta_{\rm phase} = \pm\theta_{\rm G}$, the Gendrin angle. For $0 < \theta_{\rm phase} < \theta_{\rm G}$ the wave spread is rather small ($\theta_{\rm group} < 5°$), hence amplitude decay is mostly due to damping. However, the group velocity angle becomes $\theta_{\rm group,max} \simeq -19°$ near $\theta_{\rm phase,max} = 69°$. Since the angles have opposite sign, $|\theta_{\rm phase}|+|\theta_{\rm group}| = 88°$, i.e., $\mathbf{v}_{\rm group}$ is nearly orthogonal to $\mathbf{v}_{\rm phase}$. A measurement of the group velocity is not possible with cw plane waves since $v_{\rm group} = d\omega/dk$ describes the propagation of the envelope of wave packets, e.g., formed by a beat mode with two frequencies ($\omega_1 - \omega_2 = \Delta\omega$) and two wavenumbers ($k_1 - k_2 = \Delta k$), or by a wave burst [15].

The polarization of oblique whistler modes has been described theoretically [16] but not yet shown experimentally. The vector field (B_y, B_z) is shown in Fig. 7(a) for an oblique whistler mode near the Gendrin angle. The direction of the wave magnetic field is parallel to the phase fronts such that $\mathbf{k}\cdot\mathbf{B} \simeq 0$. A hodogram of the wave magnetic field (B_x, B_y, B_z) along the direction of the oblique $\mathbf{k}$-vector is shown in Fig. 7(b). It shows that the spatial polarization is circular and left-handed, the same as for whistler propagation along $\mathbf{B}_0$. Figure 7(c) shows an end view of the hodogram along $\mathbf{k}$ which shows the left-handed rotation more obviously. The temporal polarization is right-handed.

C. Interference of oblique whistler modes

We now address the interference of two oblique plane whistler modes which can arise from specular wave reflections. Two arrays are stacked along y with their dipole moments

orthogonal to $\mathbf{B}_0$. Then one array is phased so as to produce oblique propagation at an angle $+\theta$ with respect to $\mathbf{B}_0$ and the other array excites waves at $-\theta$. The resultant interference pattern is shown in Fig. 8(a-c) for each field component as contour plots in the y–z plane. Only the left half plane of the antenna is shown since the right one is redundant.

In order to visualize the field topology, we simplify the 3D fields into linked 2D field lines as earlier done for whistler vortices. A white square of sides $\lambda/2$ is placed at the same location in each plane as a visual aid, and the field vectors are identified within the squares. Figure 8(d) shows that the out-of-plane component B_x maximizes on the corners with alternating signs and nearly vanishes in the center. The B_y and B_z components nearly vanish on the corners as well as in the center. After constructing the (B_y, B_z) field lines one identifies an X-type null in the center and an O-type null around each corner. The field line closure of the alternating B_x vectors shows that the out-of-plane lines link with the in-plane lines in a left-handed sense, implying negative magnetic helicity. This is consistent with whistler modes propagating against $\mathbf{B}_0$.

Spatial and temporal polarizations depend on position and direction of wave propagation. The spatial polarization along z is circular along the top and bottom sides of the box, but linear through the center of the box ($\pm B_z$). The temporal polarization is obtained by observing the field rotation at a fixed point as the wave passes by. For example, as the wave field shifts to the left, the field $-B_x$ at the left upper corner of the square turns into $-B_y$ and then into $+B_x$, which is a counterclockwise or right-handed rotation around $\mathbf{B}_0$ like that of the electrons. The same holds along the bottom of the box, but in the center the polarization is linear and longitudinal. This example shows again that polarization measurements from single points are not meaningful unless the wave is a single plane wave, which of course cannot be established from a single point. No evidence for a left-handed temporal polarization is observed as has been predicted theoretically for wave interference [17].

The interference of the waves results in axial wave propagation and radial standing waves, which is verified in two time-of-flight diagrams. Figure 8(e) shows that the wave propagates with axial phase velocity $v_{\mathrm{phase},\parallel} \simeq 75$ cm/μs away from the array at $z = 0$. The y–t diagram of Fig. 8(f) shows no phase shifts across $\mathbf{B}_0$, just alternating signs of $B_y(t)$, which are the properties of standing waves. The resultant wave propagation is as in a waveguide, except that the standing waves are not produced by wave reflection from conducting boundaries.

Such patterns can also arise from wave reflections of oblique whistlers at sharp gradients in the refractive index or conductivity.

IV. CONCLUSION

The properties of magnetic antenna arrays for exciting whistler modes have been investigated. The approach has been to measure the fields of one loop antenna and to construct the radiation pattern from an antenna array by linear superposition of shifted single-antenna patterns. The objective is to produce approximate plane waves which cannot be done by single antennas either small or large compared to the wavelength.

An array of closely spaced loop antennas approximates a line dipole which can be stacked onto a sheet of dipoles to produce plane phase fronts and constant amplitude. The present use of antenna arrays differs from those of free-space antenna arrays or optical gratings which are based on interference from sources spaced at least $\lambda/2$ apart. Furthermore, the anisotropy of the plasma prevents comparison with radiation in free space.

It has been shown that arrays of loops across $\mathbf{B}_0$ excite parallel phase fronts when all loops are driven in phase. This eliminates one $\mathbf{k}$ vector component and suggests that extending the array to two dimensions eliminates both components across $\mathbf{B}_0$ for exciting parallel plane whistlers. This would allow a meaningful comparison with plane wave theories of dispersion and damping which is not justified for wave packets excited by single antennas.

Antennas with directional radiation patterns have useful applications for exciting and receiving whistler modes. This has been demonstrated for two loops whose fields rotate like the whistler wave magnetic field. Likewise, two arrays can be used to produce directional radiation of plane waves.

One could tilt an array to produce oblique whistlers, but electronic steering by phasing the array is more versatile. When a constant delay is introduced from one element to the next, a wave propagates along the array. The antenna array imposes a well-defined perpendicular wave vector component resulting in an oblique whistler mode in the plasma. Its properties have been compared to theoretical predictions finding reasonably good agreements. The Gendrin mode and oblique cyclotron resonance have been excited.

Standing whistler modes have been studied for counter-propagating waves and for oblique whistler modes. Counter-propagating whistler vortices from two loop antennas propagating

along $\mathbf{B}_0$ have opposite helicities such that toroidal and poloidal fields cancel at different locations, hence form no absolute nulls or $B = 0$ nodes. The interference of two oblique plane whistler modes leads to "whistler waveguide" modes. These exhibit standing waves across $\mathbf{B}_0$ and propagation along $\mathbf{B}_0$. The interference produces field minima and maxima which propagate at a group velocity angle slightly oblique to $\mathbf{B}_0$.

The research could be extended to many other applications. For example, a curved phase front could be generated by uneven phase shifts between array elements. It can be used to focus whistlers. However, phase focusing is not the same as energy focusing which requires focusing the group velocity ray.

Using 2D phased arrays, the reflection of plane oblique whistlers from conductivity discontinuities can be studied which can produce two reflected waves. This problem arises in narrow density ducts [18], in helicon devices with glass tubes, and near lunar crustal magnetic fields where standing whistler modes have been observed [19].

Similarities to the popular helicon devices have been pointed out. Since the $m = 0$ and $m = 1$ modes are also observed in the present unbounded plasma, they are not characteristic modes of a cylindrical plasma column. However, they are whistler modes excited by loop antennas with different orientations to $\mathbf{B}_0$. When loop antennas are stacked, the $m = 1$ mode transitions into a plane wave, which is the commonly assumed whistler mode in space plasmas. However, this concept may not hold in the near-zone of an excitation region or in the presence of sharp gradients which create wave reflections. Many concepts of whistler wave theories have not and cannot be tested with single point observations in space plasmas.

Finally, it is also worth pointing out that the interpretation of diagnostic probe data should be reexamined. Typically magnetic probes in plasmas are assumed to behave as in free space but they are actually receiving antennas. In plasmas, their radiation patterns can vastly differ from that in free space, e.g., small electric dipoles [20] and magnetic dipoles [1] have radiation patterns which peak near the group velocity resonance cone given by $\sin\theta = \omega/\omega_{ce}$. Thus, a small diagnostic loop produces a larger signal for an oblique whistler mode than for a plane parallel whistler mode. Another example is a directional antenna. When used as a receiving antenna, it detects predominantly those waves which have the same helicity as the antenna. Transmission between two directional antennas is not reciprocal [21]. If a phased array were used as a receiving antenna, it would produce a peak signal for an oblique plane whistler mode rather than a parallel whistler mode. Directional receiving arrays are

more sensitive than non-directional antennas and can determine the propagation direction of plane waves without requiring electric field measurements and plane wave assumptions [22]. Thus, the receiving properties of antennas are useful but need further investigations.

Acknowledgments

The authors gratefully acknowledge support from NSF/DOE grant 20101721.

---

[1] R. L. Stenzel, Radio Sci. **11**, 1045 (1976), URL http://dx.doi.org/10.1029/RS011i012p01045.

[2] A. V. Kostrov, A. V. Kudrin, L. E. Kurina, G. A. Luchinin, A. A. Shaykin, and T. M. Zaboronkova, Phys. Scripta **62**, 51 (2000), URL http://dx.doi.org/10.1238/Physica.Regular.062a00051.

[3] M. E. Gushchin, S. V. Korobkov, A. V. Kostrov, A. V. Strikovsky, T. M. Zaboronkova, C. Krafft, and V. A. Koldanov, Phys. Plasmas **15**, 053503 (2008), URL http://dx.doi.org/10.1063/1.2907784.

[4] D. D. Blackwell, D. N. Walker, and W. E. Amatucci, Phys. Plasmas **17**, 012901 (2010), URL http://dx.doi.org/10.1063/1.3274453.

[5] H. G. James, Review of Radio Science **336**, 75 (2011).

[6] C. M. Franck, R. Kleiber, G. Bonhomme, O. Grulke, and T. Klinger, Phys. Plasmas **10**, 3817 (2003), URL http://dx.doi.org/10.1063/1.1602697.

[7] V. S. Sonwalkar, U. S. Inan, T. F. Bell, R. A. Helliwell, O. A. Molchanov, and J. L. Green, J. Geophys. Res. **99**, 6173 (1994), URL http://dx.doi.org/10.1029/93JA03310.

[8] R. W. Boswell and F. F. Chen, Plasma Science, IEEE Transactions on **25**, 1229 (1997), URL http://dx.doi.org/10.1109/27.650898.

[9] F. F. Chen and R. W. Boswell, Plasma Science, IEEE Transactions on **25**, 1245 (1997), URL http://dx.doi.org/10.1109/27.650899.

[10] G. R. Tynan, A. D. Bailey, III, G. A. Campbell, R. Charatan, A. de Chambrier, G. Gibson, D. J. Hemker, K. Jones, A. Kuthi, C. Lee, et al., J. Vac. Sci. Technol. A **15**, 2885 (1997), URL http://dx.doi.org//10.1116/1.580844.

[11] J. M. Urrutia and R. L. Stenzel, companion paper 1, submitted to Phys. Plasmas (2014), URL http://www.physics.ucla.edu/plasma-exp/references/publications/PoP/WAntennas-1.pdf.

[12] R. L. Stenzel, J. M. Urrutia, and M. C. Griskey, Phys. Scripta **T84**, 112 (2000), URL http://dx.doi.org/10.1238/Physica.Topical.084a00112.

[13] R. A. Helliwell, *Whistlers and Related Ionospheric Phenomena* (Stanford University Press, Stanford, CA, 1965).

[14] C. L. Rousculp, R. L. Stenzel, and J. M. Urrutia, Phys. Plasmas **2**, 4083 (1995), URL http://dx.doi.org/10.1063/1.871031.

[15] D. R. Baker and T. A. Hall, Plasma Physics **16**, 901 (1974), URL http://dx.doi.org/10.1088/0032-1028/16/10/002.

[16] P. M. Bellan, Phys. Plasmas **20**, 082113 (2013), URL http://dx.doi.org/10.1063/1.4817964.

[17] B. Lundin and C. Krafft, Annales Geophysicae **20**, 1153 (2002), URL http://dx.doi.org/10.5194/angeo-20-1153-2002.

[18] J. C. Lee, Int. J. Electr. **26**, 537 (1969), URL http://dx.doi.org/10.1080/00207216908938184.

[19] J. S. Halekas, D. A. Brain, D. L. Mitchell, and R. P. Lin, Geophys. Res. Lett. **33**, L22104 (2006), URL http://dx.doi.org/10.1029/2006GL027684.

[20] H. G. James, IEEE Trans. on Antennas and Propagation **48**, 1340 (2000), URL http://dx.doi.org/10.1109/8.898766.

[21] R. L. Stenzel, J. M. Urrutia, and M. C. Griskey, Phys. Plasmas **6**, 4450 (1999), URL http://dx.doi.org/10.1063/1.873731.

[22] O. Santolik, M. Parrot, and F. Lefeuvre, Radio Science **38**, 1010 (2009), URL http://dx.doi.org/10.1029/2000RS002523.

Figures

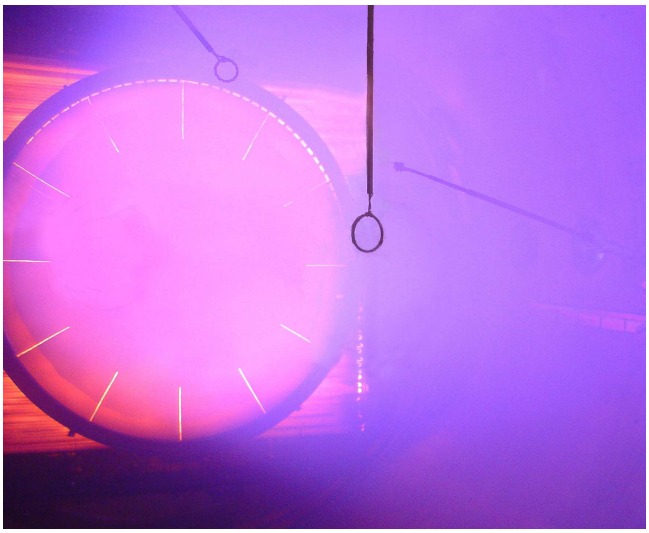

FIG. 1: Photograph of the discharge plasma source using a 1 m diam oxide coated cathode. A 4 cm diam loop antenna is inserted into the uniform plasma center to excite low frequency whistler modes (vertical probe shaft). The topology of the wave field is measured with a three-component magnetic probe movable in three dimensional space (right probe shaft). By superimposing shifted patterns from the single antenna, the radiation properties of antenna arrays are obtained.

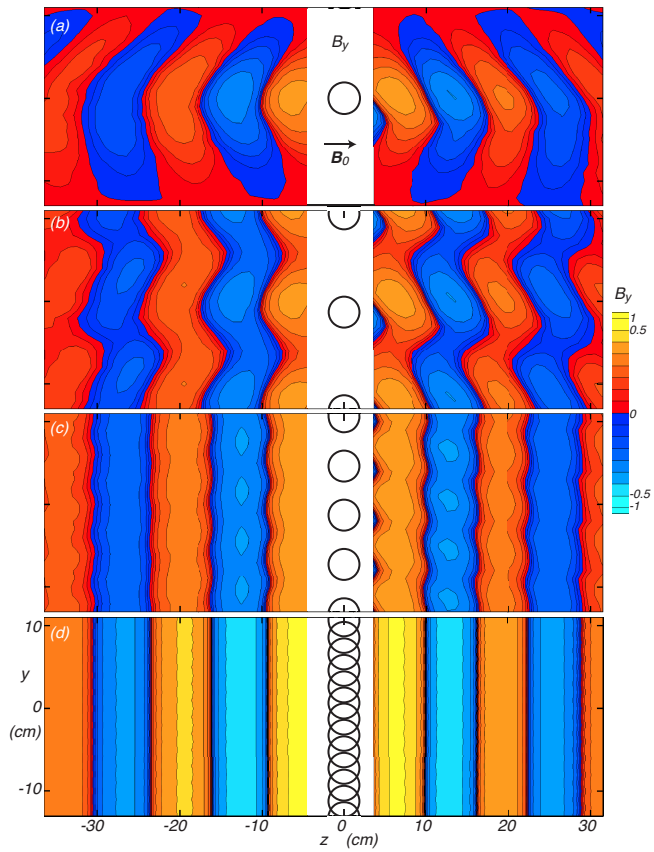

FIG. 2: Snapshots of the transverse magnetic field $B_y(0, y, z)$ from (a) widely separated loop antennas, and (b-d) decreasingly separated loops. Wide separation essentially excites waves with V-shaped phase fronts which propagate to both sides mainly along the dc magnetic field $\mathbf{B}_0$. Decreasing the antenna separation across $\mathbf{B}_0$ from (a) 12 antenna radii to (b) six yields rippled surfaces. Decreasing antenna separation even further reduces the ripples in the phase fronts resulting in (d) nearly plane waves propagating along $\pm\mathbf{B}_0$.

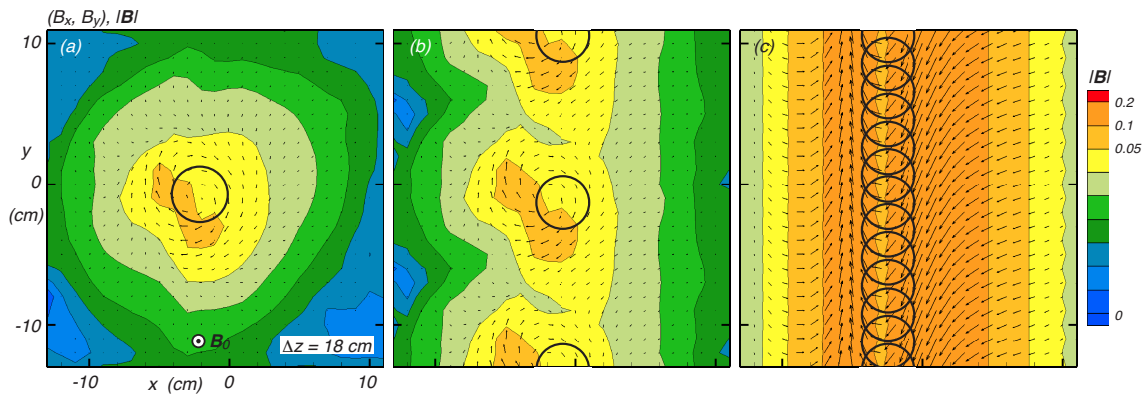

FIG. 3: Fields generated at a transverse x–y plane situated at $z = 18$ cm from antenna arrays consisting of loops whose dipole moments are oriented along $\mathbf{B}_0$. Vectors of the transverse field and contours of the total field magnitude are shown for antenna separation of (a) 12, (b) six and (c) one antenna radii. Closely spacing the antennas produce nearly constant phases along the antenna array, i.e., $k_y = 0$. Stacking arrays also in x-direction would excite plane waves with wave vector $\mathbf{k} \simeq (0, 0, k_z)$.

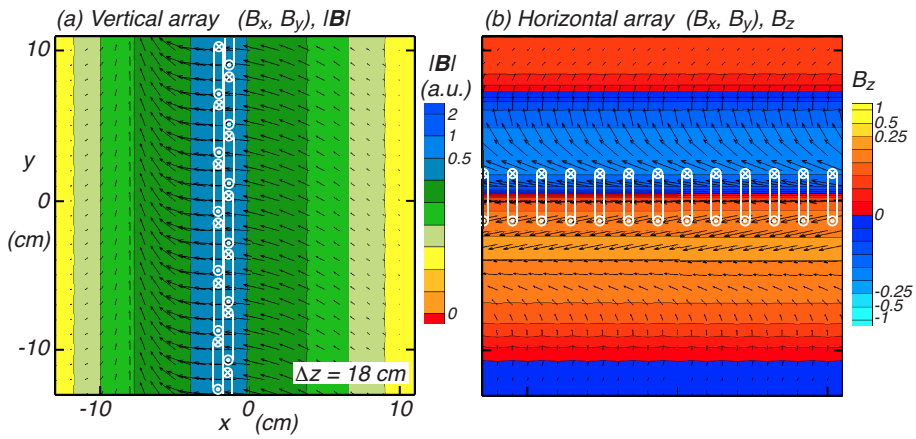

FIG. 4: Wave fields from two linear loop arrays in the x–y plane at $\Delta z = 18$ cm from the antennas whose dipole moment is in the x-direction. (a) The array is aligned with the y-axis producing a field independent of y ($k_y = 0$). Contour and vector plots show that the field amplitude is strongest in the center and points predominantly in $-x$ direction, although it rotates counterclockwise in time. (b) The array is aligned with the x-axis producing a field independent of x ($k_x = 0$). Contour plots show that $B_z \simeq 0$ near the array. If multiple vertical (horizontal) arrays are stacked horizontally (vertically), the two-dimensional array would produce whistler modes with $k_x = k_y \simeq 0$ and $B_z \simeq 0$, i.e., a plane parallel whistler mode.

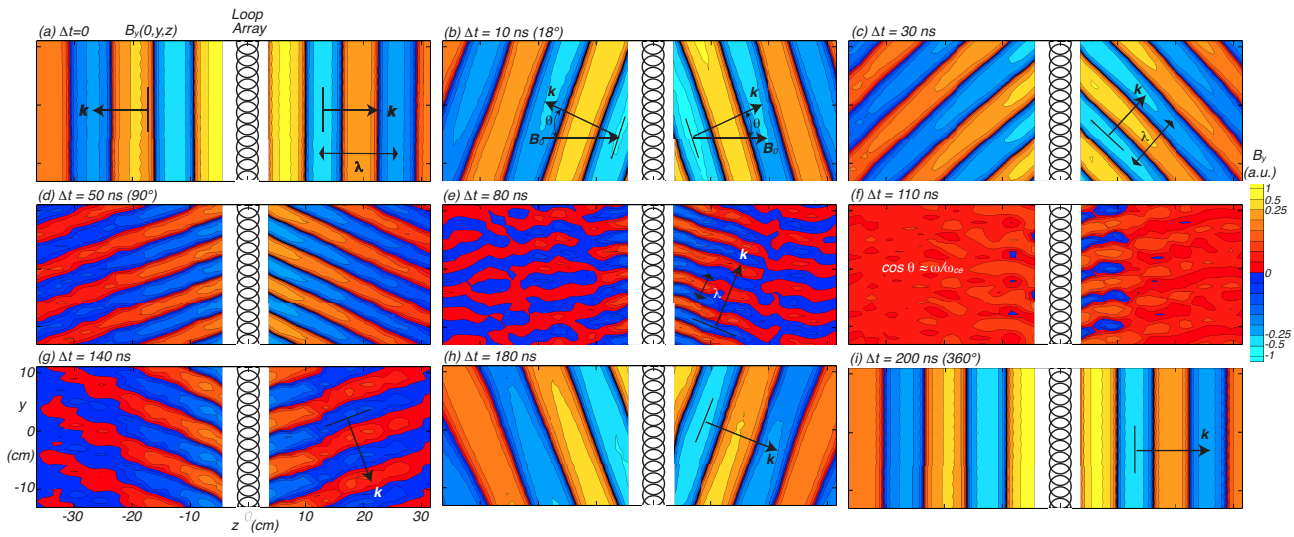

FIG. 5: The effect of phasing an antenna array which consists of antennas separated by one antenna radii whose dipole moments are across $\mathbf{B}_0$. Delaying consecutive antenna signals by a time interval Δt inclines the phase fronts, or propagation angle θ, with respect to $\mathbf{B}_0$. The angle increases as the wave phase velocity $v_y = \Delta y/\Delta t$ decreases (a–d). Oblique propagation of whistler modes is demonstrated. As the propagation angle approaches the resonance cone angle, $\theta = \arccos(\omega/\omega_{ce}) \simeq 69°$, the wave amplitude vanishes (e, f). Further delay increases the angle to $\theta > 90°$, i.e., the wave propagates downward (g, h) and eventually again along $\mathbf{B}_0$ (i).

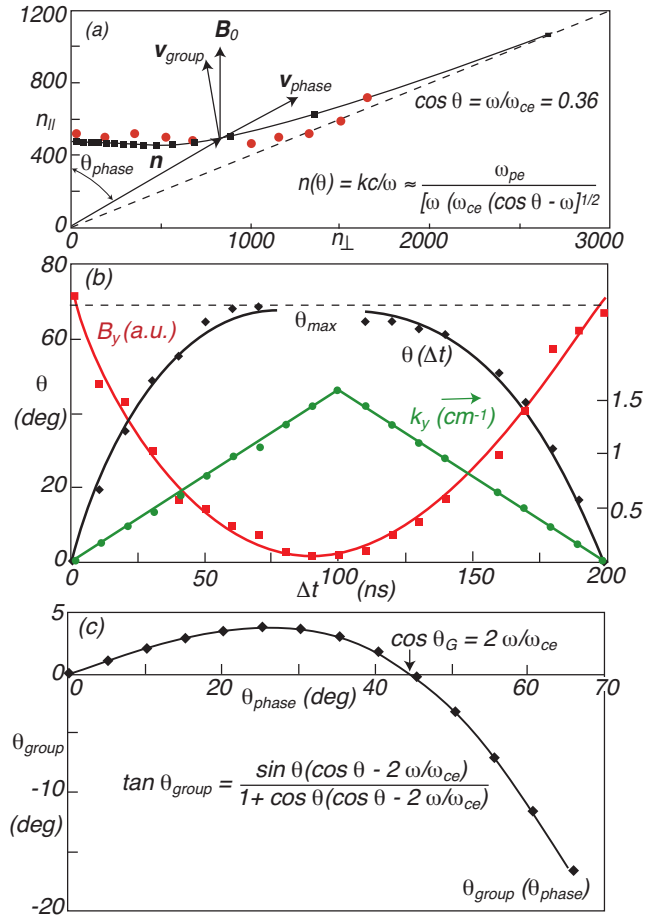

FIG. 6: Properties of oblique plane whistler modes and experimental data. (a) Refractive index surface $n(\theta)$ from theory and experimental data (red dots). In general, phase and group velocities have different angles with respect to $\mathbf{B}_0$. A dashed line indicates the oblique cyclotron resonance. (b) Observed dependence of (i) the wavenumber k_y, (ii) the propagation angle $\theta_{\rm phase}$, and (iii) the wave amplitude on the delay time between adjacent loops in the antenna array. (c) Theoretical group velocity angle vs phase velocity angle for the present experimental conditions. The Gendrin mode at $\theta_{\rm G}$ has a parallel group velocity equal to the parallel phase velocity but a highly oblique phase velocity. Energy spread becomes significant near the resonance cone angle $\theta_{\rm max} \simeq 69°$.

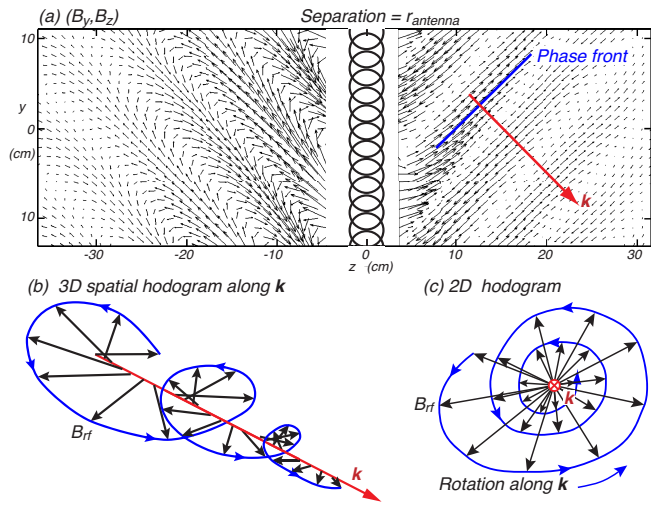

FIG. 7: Polarization of oblique whistler waves. (a) Vector field of an obliquely propagating whistler mode excited by an array of 12 delayed loops antennas. The phase front and orthogonal wave vector $\mathbf{k}$ are indicated. (b) Hodogram of the wave magnetic field $\mathbf{B}_{\rm rf} = (B_x, B_y, B_z)$ along $\mathbf{k}$. The vector rotation is left-handed which is clearly seen when $\mathbf{B}$ is displayed in a plane normal to $\mathbf{k}$ (c). This is the correct polarization for whistlers, even for oblique propagation.

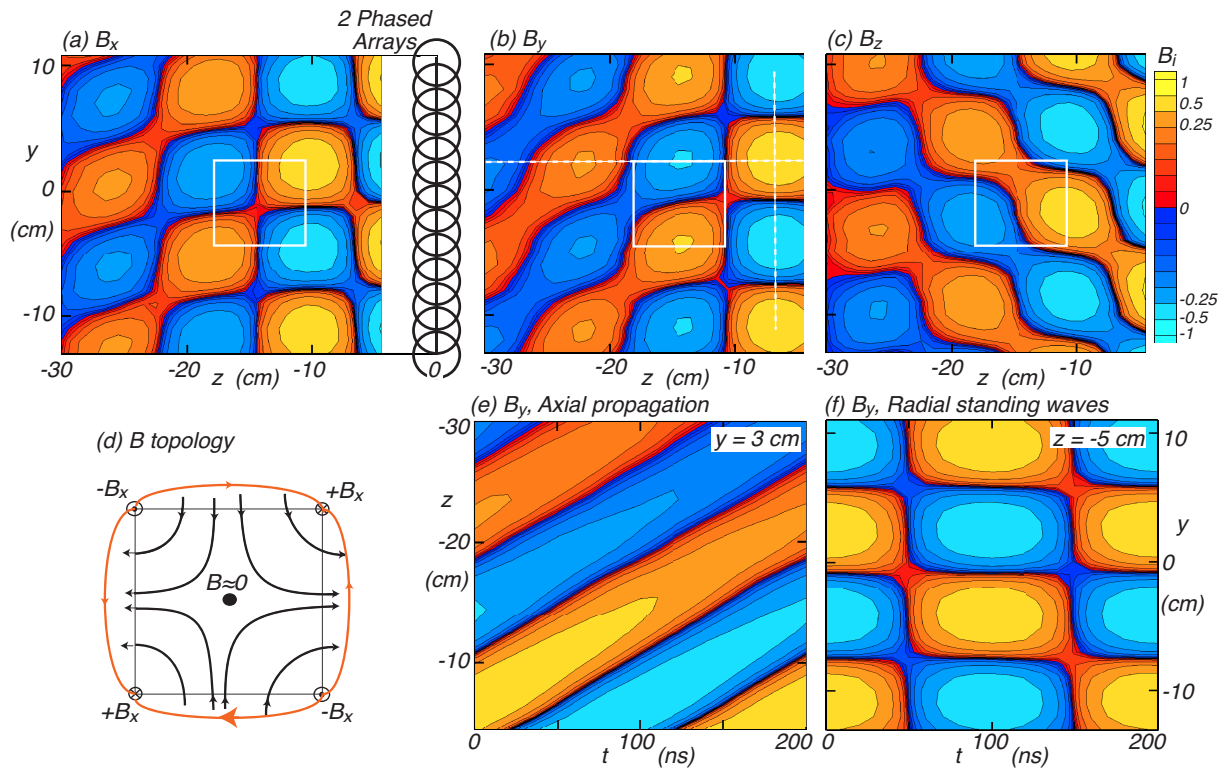

FIG. 8: Interference of two oblique whistler modes resulting in "whistler waveguide" modes. The waves are excited with two arrays along y located at $z = 0$. By delaying each array differently, two oblique waves with different propagation vectors $\mathbf{k}$ are produced, chosen to be at $\theta \simeq \pm 45°$. Displayed are contours of the three field components (a-c) in the y–z plane to the left of the array. The field topology is displayed schematically in (d). It is derived from the vector components in the white squares of sides $\lambda/2$ shown in (a-c). The field lines (B_y, B_z) exhibit an X-type null point in the center of the square and O-points around each corner where B_x has extrema. The closure of the B_x lines links with the (B_y, B_z) lines which implies magnetic helicity. The linkage is left-handed, i.e., the helicity is negative consistent with propagation against $\mathbf{B}_0$. (e) A z–t diagram of B_y shows that the wave propagates axially. (f) A y–t diagram of B_y at $z = -5$ cm [see dashed line in (b)] shows standing waves across $\mathbf{B}_0$. Such modes can arise from oblique reflections.